Palaeogeography, Palaeoclimatology, Palaeoecology 502 (2018) 119–129

Contents lists available at ScienceDirect

Palaeogeography, Palaeoclimatology, Palaeoecology

journal homepage: www.elsevier.com/locate/palaeo

Direct and indirect effects of Holocene climate variations on catchment and lake processes of a treeline lake, SW China

Xu Chen[a,*], Suzanne McGowan[b], Xiayun Xiao[c], Mark A. Stevenson[d], Xiangdong Yang[c], Yanling Li[c], Enlou Zhang[c]

[a] State Key Laboratory of Biogeology and Environmental Geology, School of Earth Sciences, China University of Geosciences, Wuhan, China
[b] School of Geography, University of Nottingham, Nottingham, NG7 2RD, UK
[c] State Key Laboratory of Lake Science and Environment, Nanjing Institute of Geography and Limnology, Chinese Academy of Sciences, Nanjing, China
[d] School of Natural and Environmental Sciences, Newcastle University, Newcastle-upon-Tyne, NE1 7RU, UK

ARTICLE INFO

Keywords:
Climate change
Chlorophyll and carotenoid pigments
Sediment geochemistry
Erosion
Soil formation
Lake ontogeny

ABSTRACT

Sedimentary records of inorganic elements and pigments over the last 12,000 years are used to assess major changes in limnological conditions of Tiancai Lake (a small treeline lake, SW China), in response to Holocene climate variations. Algal communities shifted from the dominance of cyanobacteria and cryptophytes in the early Holocene, towards siliceous algae in the mid-Holocene and chlorophytes in the late Holocene. Algae responded to a combination of climate-mediated vegetation and soil development associated with allochthonous inputs of dissolved nutrients and organic matter, and sediment infilling. Decreases in Al, Pb, Cu and Zn from the early Holocene probably resulted from soil podsolization and the sequestration of these elements within soils. Changes in Mn and Fe were likely linked to redox condition in catchment soils and water column. Synchronous peaks in Ti, Ba, Ca, Sr, Na, K and Mg, median grain size and magnetic susceptibility coincided with the troughs in the chemical index of alteration, indicating that episodic cold events enhanced upland bedrock erosion and transported unleached and coarse detritus into the lake. These cold events broadly correlate with Holocene ice-rafting events in the North Atlantic. Although the cold events altered the influx of minerogenic elements by regulating upland bedrock erosion, climate-mediated vegetation and soil development led to a muted impact on primary producers. Holocene algal community shifts were subtle, reflecting the relative abundance of P (derived from weathering) and N (derived from soils) throughout the record, with the most pronounced effects on the lake biota being benthic expansion which occurred in response to sediment infilling.

1. Introduction

Treeline lakes located close to ecotonal boundaries are highly sensitive to climate change as small variations in climate can give rise to large transitions in catchment vegetation and runoff, thereby influencing lake functioning (Battarbee et al., 2002; Lotter and Birks, 2003; Catalan et al., 2013). In alpine/boreal regions where the bedrock is depleted in base cations, long-term catchment development and ontogeny generally cause lakes to become acidic and dilute, as the influx of organic matter increases and mineral leaching declines with soil development (Engstrom et al., 2000; Fritz et al., 2004; Fritz and Anderson, 2013; Lu et al., 2017). Given that key nutrients (phosphorus and bases such as Ca) for alpine lakes come largely from bedrock weathering (Boyle et al., 2013), mineral depletion after glacial retreat can trigger ecosystem succession (Engstrom et al., 2000). Generally, the initial alkaliphilous diatom species of the late-glacial are replaced by acidophilous taxa in boreal lakes (Pennington et al., 1972; Renberg, 1990; Bradshaw et al., 2000).

Alpine lakes in southwestern China, close to the Tibetan Plateau, are strongly influenced by the Asian monsoon. Sedimentary records in these lakes can provide long-term insights into past climate dynamics over Southeast Asia (Xiao et al., 2014; Wang et al., 2016a; Zhang et al., 2017; Li et al., 2018), with important socio-economic or environmental ramifications (Wang et al., 2005). Generally, the weak Asian monsoon during the late-glacial was replaced by a more intensified monsoon after the onset of the Holocene. Warm and wet conditions persisted until ca. 4.5–5.0 cal kyr B.P. when monsoon strength started to weaken up to the present day (Dykoski et al., 2005; Wang et al., 2005). Holocene climate change is known to regulate catchment vegetation and soil development, subsequently influencing aquatic ecosystems (Xiao et al., 2014; Wang et al., 2016a). Major changes in sedimentary diatom assemblages in southwestern China generally correspond with the broad

* Corresponding author.
E-mail address: xuchen@cug.edu.cn (X. Chen).

https://doi.org/10.1016/j.palaeo.2018.04.027
Received 16 February 2018; Received in revised form 15 April 2018; Accepted 16 April 2018
Available online 04 May 2018
0031-0182/ © 2018 Elsevier B.V. All rights reserved.

trend of Holocene monsoonal variations, mainly linked to climate-mediated catchment processes (Chen et al., 2014; Wang et al., 2016a; Li et al., 2018).

Besides the general trend, Holocene climate variations are characterized by several rapid cooling events in southwestern China lasting several centuries in duration (Hong et al., 2003; Morrill et al., 2003; Mayewski et al., 2004; Wang et al., 2005; Wang et al., 2016b; Ning et al., 2017). Cold events are inferred from lake sediment characteristics such as rapid declines in the proportion of organic matter and changes in grain size and weathering indicators, which suggest an increase in erosion of unweathered material into lake basins (Mischke and Zhang, 2010). Cold events may be associated with prolonged snow-cover, accelerated upland bedrock erosion, and elevated influx of detritus and base cations to lakes (Koinig et al., 2003; Schmidt et al., 2006; Mischke and Zhang, 2010). Changes in terrestrial influxes are known to alter limnological conditions and biotic communities in lakes (Likens and Bormann, 1974; Leavitt et al., 2009). However, the effects of Holocene cooling events on alpine lake ecosystems in the monsoon-influenced regions have rarely been assessed.

Sedimentary pigments and inorganic elements were analysed from Tiancai Lake, located at treeline in Yunnan Province (SW China). Sedimentary chlorophylls and carotenoids can be used to infer past algal communities (Leavitt and Hodgson, 2001; McGowan, 2013), whereas inorganic elements can provide information about catchment processes such as bedrock erosion and soil formation (Boyle, 2001; Koinig et al., 2003; Schmidt et al., 2006; Lu et al., 2017). This study presents sedimentary element and pigment records in Tiancai Lake over the last 12,000 years, combined with previously published pollen and diatom data from the same site (Chen et al., 2014; Xiao et al., 2014), in order to reveal the linkages between the terrestrial and aquatic ecosystems, and their co-evolution in response to Holocene climate variations.

2. Materials and methods

2.1. Study area

Tiancai Lake (26°38′3.8″N, 99°43′00″E; 3898 m a.s.l.) has a surface area of ~2.1 ha, a mean depth of 6 m and is located on granite bedrock at the northeastern slope of the Laojun Mountains (summit ~4200 m a.s.l.), which is located at the southeastern edge of the Tibetan Plateau, SW China (Fig. 1A and B). The chemical composition of the bedrock is characterized by high proportions of SiO_2 (71.3–73.4%) and total alkali (K_2O + Na_2O, 7.4–8.8%) (Ma, 2013). The climate in this region is strongly influenced by the Asian monsoon, with a mean annual temperature of ~12.7 °C and mean annual precipitation of ~970 mm at Lijiang City (nearby meteorological station; 2393 m a.s.l.; Fig. 2). Primary forest around the lake appears to be undisturbed, and is characterized by montane conifers such as *Abies georgii*, with the timberline at about 4000 m a.s.l. (Fig. 1C). The upper catchment above the timberline is mainly composed of alpine *Rhododendron* shrubland, *Kobresia* meadow and alpine tundra. Soil type in the catchment is a brown podzolic soil, with a mean pH of 4.03, organic matter of 177 mg g^{-1}, total nitrogen of 11 mg g^{-1}, total phosphorus of 1 mg g^{-1} and total potassium of 10 mg g^{-1} (Shi, 2007). The lake is hydrologically open with the inflow from the south and an outflow to the north (Fig. 1C). The lake water is brown-coloured, with a pH of 7.91, total nitrogen of 0.5 mg L^{-1}, total phosphorus of 14 μg L^{-1}, and dissolved organic carbon (DOC) of 10 mg L^{-1} measured in June 2013 (Du et al., 2016).

2.2. Sample collection and laboratory analysis

A 926-cm-long core was extracted from the centre of the lake in 2008 at a water depth of 6.8 m using a Uwitech Coring Platform System, and sectioned at 1-cm intervals. Sediments in this core consist of alternate dark gyttja and dark silty gyttja, i.e., black gyttja between 926 and 820 cm, 817 and 692 cm, 587 and 358 cm, 341 and 321 cm, 319 and 96 cm with dark silty gyttja in the intervals; and black gyttja with many plant remains in the uppermost 96 cm. The age-depth model of Tiancai Lake is published in Xiao et al. (2014) based on a best-fit second order polynomial function derived from 18 calibrated radiocarbon dates. In this study, an updated age model was developed based on the same 18 radiocarbon dates using the Bayesian model (Bacon 2.2) in R language (Blaauw and Christen, 2011). Bacon repeatedly samples from the probability density function of each calibrated age, fits many possible splines to the age-depth data, and rejects fitted splines that give rise to age reversals. Default settings were used when calculating the age-depth model. All ages are reported in calendar years before radiocarbon present (1950 CE).

A total of 100 subsamples taken from the Tiancai Lake core at ~10-cm intervals were used for laboratory measurements. For elemental analyses, the freeze dried samples (~125 mg) were completely digested with a mixture of four acids (i.e., HF, HCl, HNO_3 and $HClO_4$) and prepared for the measurement of Al, Ba, Ca, Sr, Na, K, Mg, Ti, Mn, Fe, P, Pb, Cu and Zn by inductively coupled plasma-atomic emission spectrometry (ICP-AES) with SPEX™ from the US as the standard solution (± 2%). Quality control was assured by the analysis of duplicate samples, blanks, and reference materials (GSD-9 and GSD-11, Chinese geological reference materials). The reproducibility of the duplicated sediment samples was > 90% for all elements. Blank digestion solution results were < 5% for all samples and elements, and all standard deviations in prepared samples were < 7% of documented certified values.

For pigment analyses, freeze-dried weighed sediments (~200 mg) were extracted in a mixture of acetone:methanol:water (80:15:5) by leaving in a − 20 °C freezer for 24 h. Extracts were filtered with a 0.22-μm-pore PTFE filter, dried under N_2 gas, re-dissolved in an acetone:ion-pairing reagent:methanol mixture (70:25:5) and then injected into an Agilent 1200 series high performance liquid chromatography unit (HPLC). The separation conditions with quaternary pump, autosampler, ODS Hypersil column (250 × 4.6 mm; 5 μm particle size) and photodiode array detector followed a modification of Chen et al. (2001). Pigments were identified and quantified based on their retention time and absorption spectra, compared with commercial pigment standards from DHI, Denmark (Leavitt and Hodgson, 2001; McGowan, 2013). The analysed pigments included those from all algae and plants (*β*-carotene, Chl *a*, pheophytin *a*), chlorophytes (Chl *b*, pheophytin *b*, lutein), cyanobacteria (canthaxanthin, zeaxanthin), siliceous algae (diatoxanthin) and cryptophytes (alloxanthin). Lutein and zeaxanthin did not separate in this study and so were reported here together. All concentrations were expressed as $nmol^{-1}$ g organic carbon.

2.3. Data analysis

The chemical index of alteration (CIA) was used to evaluate the weathering intensity of minerals in the sediment (Nesbitt and Young, 1982).

$$CIA = \frac{Al_2O_3}{(Al_2O_3 + K_2O + Na_2O + CaO)} \times 100 \quad (1)$$

where elemental abundances are expressed as molar proportions. A CIA value of 100 indicates intense chemical weathering along with complete removal of all the alkali (oxidation state +1) and alkaline (oxidation state +2) earth elements, whereas CIA values of 45–55 indicate less weathering.

Zonation schemes were developed for pigments and elements using the broken-stick model (Bennett, 1996) using stratigraphically constrained cluster analysis (CONISS) in the Tilia program (Grimm, 1991). Principal components analysis (PCA) was used to summarise the major underlying changes in each stratigraphical dataset because the gradient lengths of both pigment and element data, as assessed by earlier

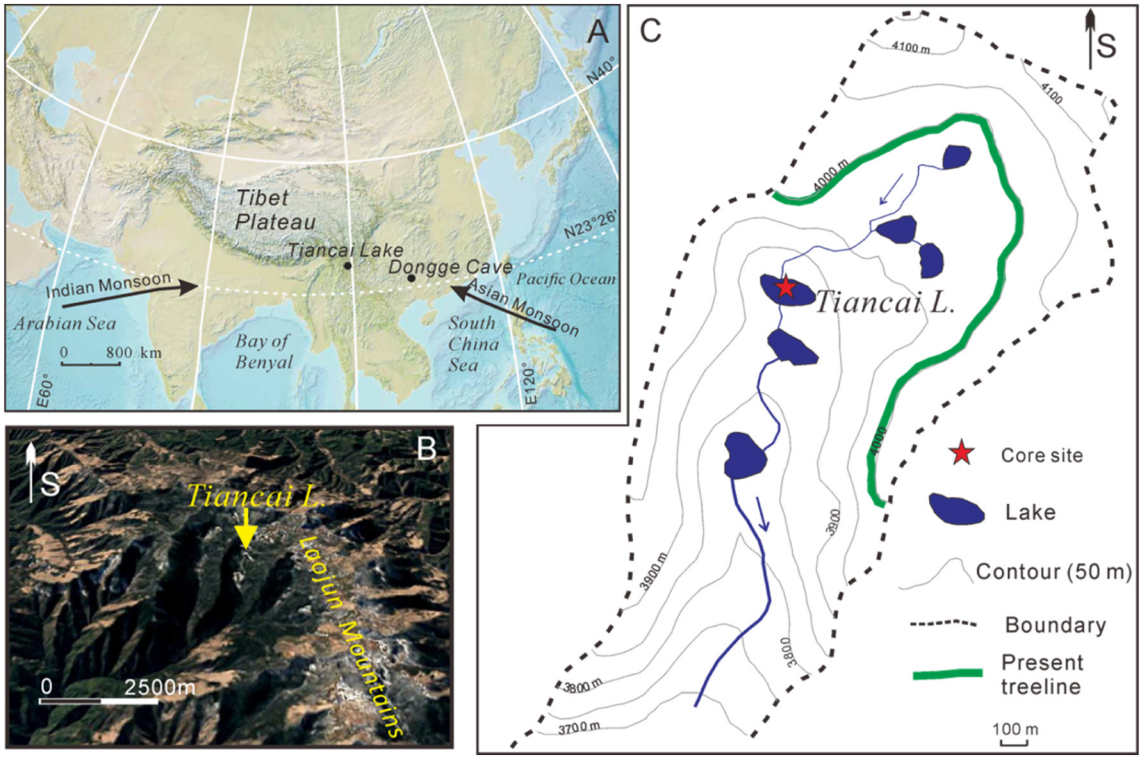

Fig. 1. Maps showing the location of Tiancai Lake in Asia relative to monsoonal pathways (A) and in the Laojun Mountains (B), and topography of Tiancai Lake catchment (C). Maps A and B have been modified from the maps downloaded from http://www.lib.utexas.edu/maps/asia.html and Google Earth (imagery captured on December 31, 1994), respectively.

detrended correspondence analysis (DCA), were < 1 standard deviation (Šmilauer and Lepš, 2014). Ordination analyses were performed on log (x + 1)-transformed pigment data and square-root transformed element data.

In order to understand the driving forces for environmental changes in Tiancai Lake, pigment and element data were compared with previously published datasets, including sedimentary records from the same sediment core: median grain size, magnetic susceptibility (χ_{lf}), TN, TOC, *Aulacoseira alpigena* relative abundance (an indicator for alkaline condition) and the percentage of *Tsuga* (a proxy for forest development) (Han et al., 2011; Chen et al., 2014; Xiao et al., 2014); and global climatic records: Dongge Cave $\delta^{18}O$ values (Dykoski et al., 2005), hematite-stained grain in the eastern North Atlantic (Bond et al., 2001), potassium ion content proxy from Greenland ice cores at GIPS2 (Mayewski et al., 2004).

Redundancy analysis (RDA) was conducted to evaluate the relationship between pigments/elements and explanatory variables from the abovementioned datasets. In addition, sediment depth was added as an explanatory variable in order to assess the influence of lake infilling on environmental changes of Tiancai Lake. Forward selection, with the false discovery rate (FDR) correction, and Monte Carlo tests (p < 0.05, n = 499 unrestricted permutations) were used to determine a minimum subset of explanatory variables. The real correlation between response variables and each significant explanatory variable was tested by the single variable partial redundancy analysis, where the rest of the significant variables were selected as co-variables. All ordinations were performed using CANOCO 5.0 (Šmilauer and Lepš, 2014).

3. Results

3.1. Chronology

The relationship between age and depth is shown in Fig. 3. The basal age of the core is ca. 11,943 ± 261 cal yr B.P. The sedimentation rate in Tiancai Lake core is rather uniform, with a mean value of ca. 0.77 mm year^{-1}. Comparison of the Bayesian model (produced in Bacon) with the polynomial fitted model (Xiao et al., 2014), shows that they are in close alignment (r = 0.999, p < 0.001). The average

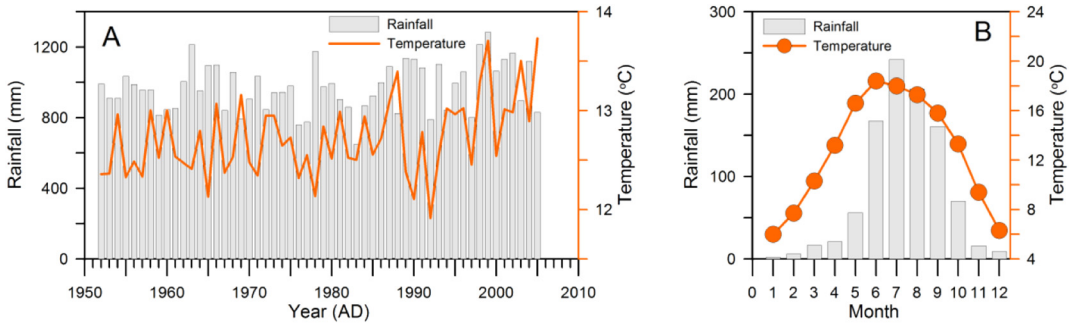

Fig. 2. Mean annual temperature and rainfall (A) and monthly temperature and rainfall (B) at Lijiang meteorological station (26°52′N, 100°13′E, 2393 m a.s.l.; 56 km away from Tiancai Lake).

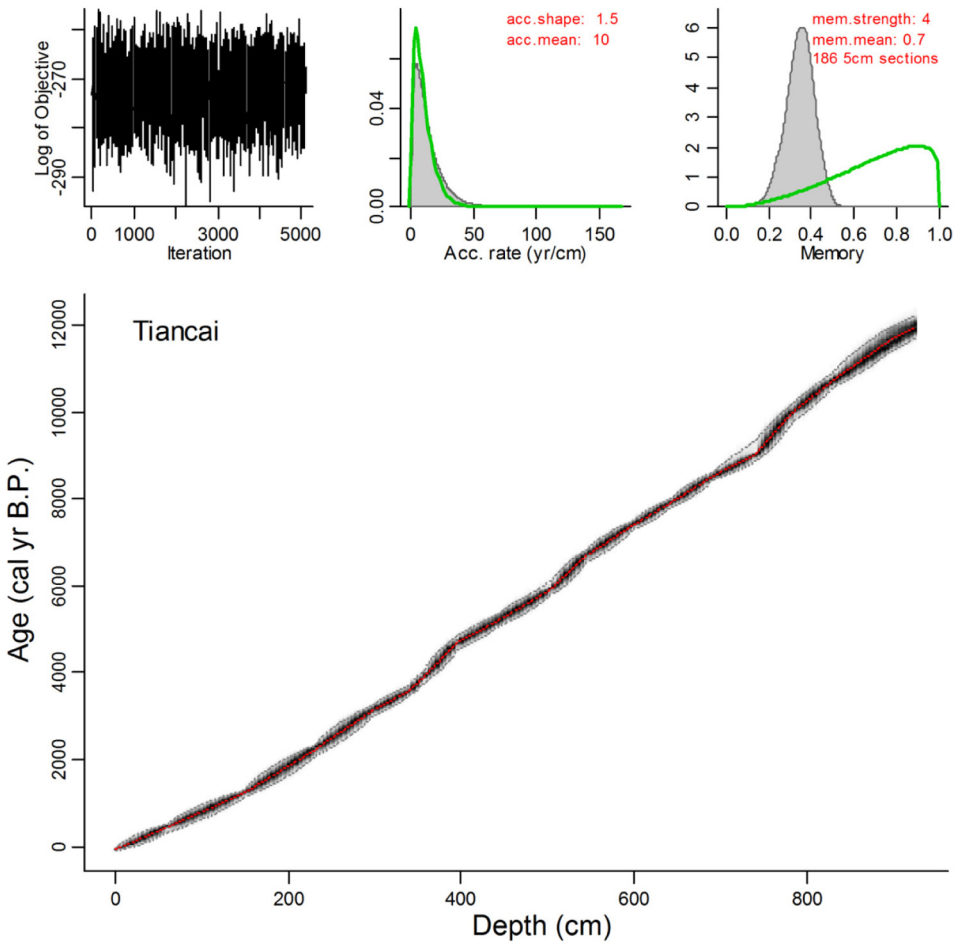

Fig. 3. Age-depth model for Tiancai Lake. Grayscale cloud represents age model probability and is bounded by a dotted-line confidence interval (95%); the darkest grey colour indicates the highest probability age for that depth. The red line shows the weighted mean age-depth model. (For interpretation of the references to colour in this figure legend, the reader is referred to the web version of this article.)

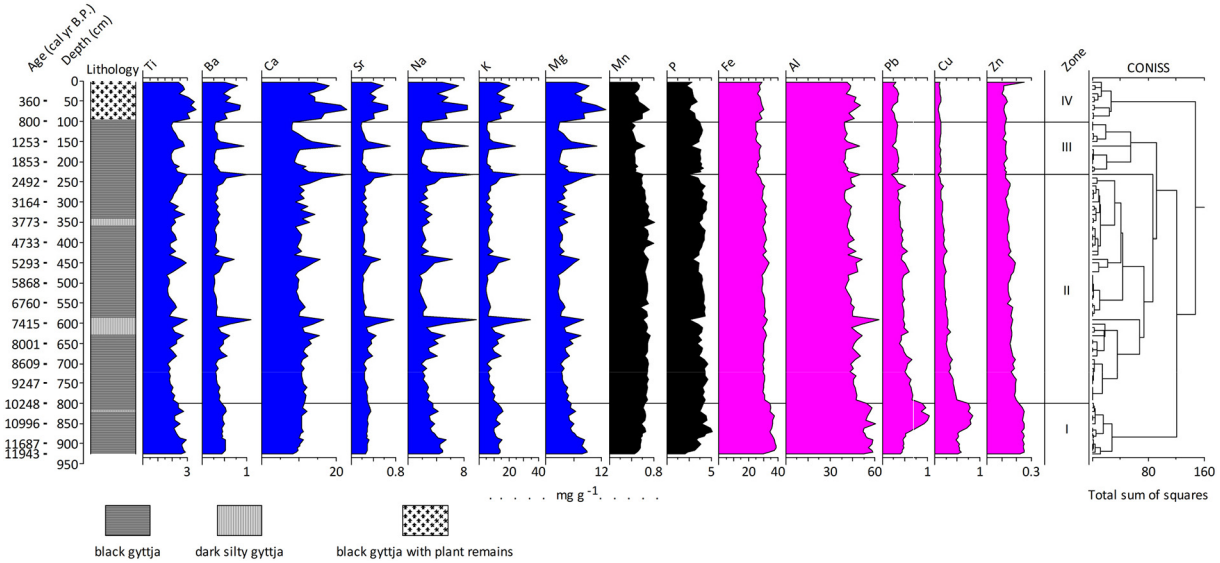

Fig. 4. Sedimentary element concentrations for the Tiancai Lake core. The number of statistically significant zones was assessed using the broken stick model (Bennett, 1996).

temporal resolution for pigment and element samples is ~119 years.

3.2. Sedimentary elements

Three distinct trends are observed in the element record (Fig. 4). Concentrations of Fe, Al, Pb, Cu and Zn were highly correlated ($r > 0.53$, $p < 0.01$) and showed general declining trends after temporary increases at the bottom of the core. The second group consists of Ti, Ba, Ca, Sr, Na, K and Mg, which were strongly correlated ($r > 0.71$, $p < 0.01$) and displayed high fluctuations, especially in the mid-to-late Holocene. Mn and P increased in the early Holocene stages and retained high values in the mid-Holocene, followed by decreasing trends in the late Holocene.

Stratigraphic element concentrations were split into four significant zones indicated by CONISS (Fig. 4). Zone I (925–801 cm; 11,943–10,263 cal yr B.P.) was characterized by the highest levels of Fe, Al, Pb, Cu and Zn. Concentrations of Ti, Na, K and Mg declined, and Mn and P concentrations increased. Concentrations of Ba, Ca and Sr were quite stable. In Zone II (801–232 cm; 10,263–2245 cal yr B.P.), Al, Pb, Cu and Zn declined whereas there were several synchronous peaks in Ti, Ba, Ca, Sr, Na, K and Mg centred at around 8390, 7773, 7297, 5191, 3491 and 2245 cal yr B.P., respectively. Concentrations of Mn, P and Fe maintained relatively high values, with slight fluctuations.

In Zone III (232–102 cm; 2245–817 cal yr B.P.), Ti, Ba, Ca, Sr, Na, K, Mg and Al were variable, with one synchronous peak centred at around 1385 cal yr B.P., accompanied by two troughs in P. Both Mn and Fe declined clearly, while Pb, Cu and Zn retained low concentrations. In Zone IV (102–0 cm; 817 cal yr B.P. to present), concentrations of Ti, Ba, Ca, Sr, Na, K and Mg increased to high levels, with one synchronous peak centred at around 541 cal yr B.P. Pb, Cu and Zn were relatively stable and retained low values. P showed a declining trend, while Mn, Fe and Al increased slightly in comparison with Zone III.

3.3. Sedimentary pigments

CONISS divided the stratigraphic pigment record into four zones (Fig. 5). In Zone I (925–861 cm; 11,943–11,152 cal yr B.P.) the cryptophyte pigment alloxanthin was abundant, and maximum abundance of the cyanobacterial pigment canthaxanthin was recorded alongside. High abundances of lutein-zeaxanthin (from chlorophytes and cyanobacteria) and β-carotene (ubiquitous in algae but often particularly abundant in cyanobacteria) were observed. In contrast, pigments from chlorophytes (Chl *b*, pheophytin *b*) and siliceous algae (diatoxanthin) were present in low abundances and concentrations of pigments from all algae (Chl *a*, pheophytin *a*) were moderate.

In Zone II (861–291 cm; 11,152–3054 cal yr B.P.) concentrations of pigments from cryptophytes (alloxanthin) and cyanobacteria (canthaxanthin and zeaxanthin) decreased slightly, but those from siliceous algae and all algae (β-carotene, Chl *a* and pheophytin *a*) increased with a notable maximum at around 8500 cal yr B.P. Pigments from chlorophytes (Chl *b* and pheophytin *b*) displayed no directional trend.

Zone III (291–81 cm; 3054–631 cal yr B.P.) was characterized by increasing concentrations of chlorophylls and derivatives, including Chl *b* and pheophytin *b* (from chlorophytes) and Chl *a* and pheophytin *a* (from all primary producers). The abundance of diatoxanthin from siliceous algae was variable but high, whereas there were decreases in cyanobacteria (canthaxanthin) and cryptophytes (alloxanthin).

In Zone IV (81–0 cm; 631 cal yr B.P. to present) pigment assemblages were markedly different from other zones. Concentrations of chlorophytes and total algal pigments were much higher (Chls *a* and *b*, pheophytins *a* and *b*), and abundances of pigments from siliceous algae (diatoxanthin), cryptophytes (alloxanthin) and cyanobacteria (canthaxanthin) were lower.

3.4. Multivariate analysis

For the elemental data, the first two PCA axes captured 93.5% of the total variance (Fig. 6A). PCA axis 1 ($PCA1_{elements}$) was positively correlated with K, Mg, Ba, Na, Ti, Sr and Ca, while PCA axis 2 ($PCA2_{elements}$) was positively related to Cu, Pb, Zn, Fe, Al and Mn (Fig. 6A). For pigments, PCA axis 1 ($PCA1_{pigments}$) explained 51.4% of the total variance and was strongly correlated with chlorophylls and their derivatives from chlorophytes (Chl *b* and pheophytin *b*) and all primary producers (Chl *a* and pheophytin *a*) (Fig. 6B). PCA axis 2 ($PCA2_{pigments}$) explained a further 22% of the variance in the pigment assemblages and was correlated with carotenoids from chlorophytes/cyanobacteria (lutein-zeaxanthin), siliceous algae (diatoxanthin), cyanobacteria (canthaxanthin) and cryptophytes (alloxanthin).

$PCA1_{elements}$ correlated with CIA, median grain size, magnetic susceptibility, TOC and TN (Fig. 7A–F). In addition, seven visible oscillations in physical and geochemical records of Tiancai Lake can be correlated within the radiocarbon age uncertainties to the North Atlantic

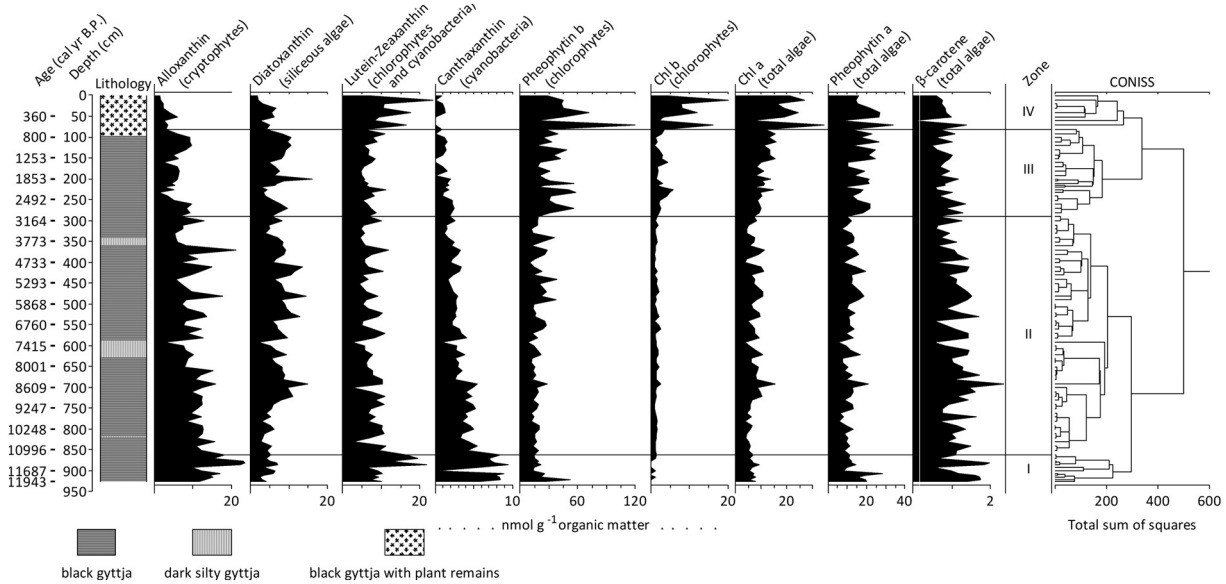

Fig. 5. Fossil pigment diagram of the Tiancai Lake core, with pigment affinity given in parentheses. The number of statistically significant zones was assessed using the broken stick model (Bennett, 1996).

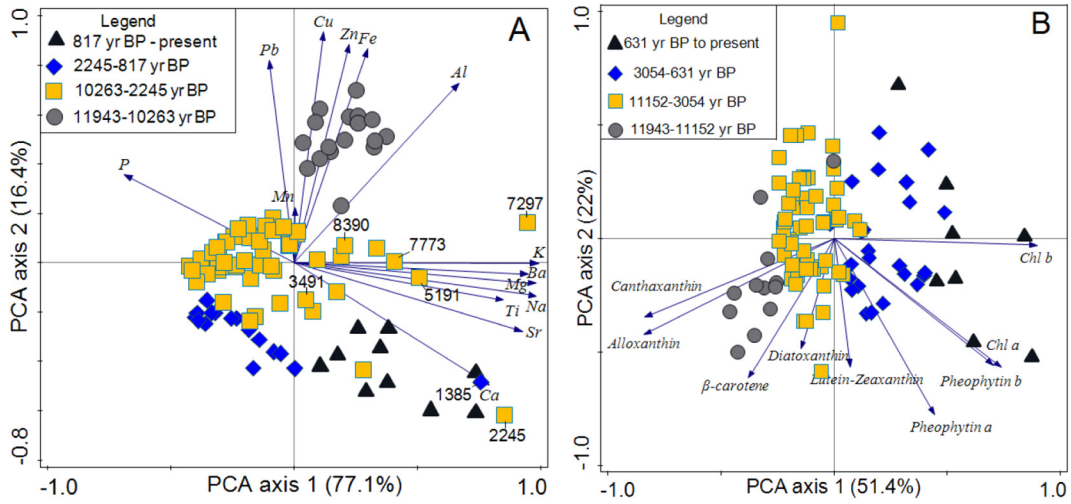

Fig. 6. Principal components analyses of elements (four zones correspond to those in Fig. 4; A) and pigments (four zones correspond to those in Fig. 5; B). Cold events are labelled with their age in panel A in cal yr B.P.

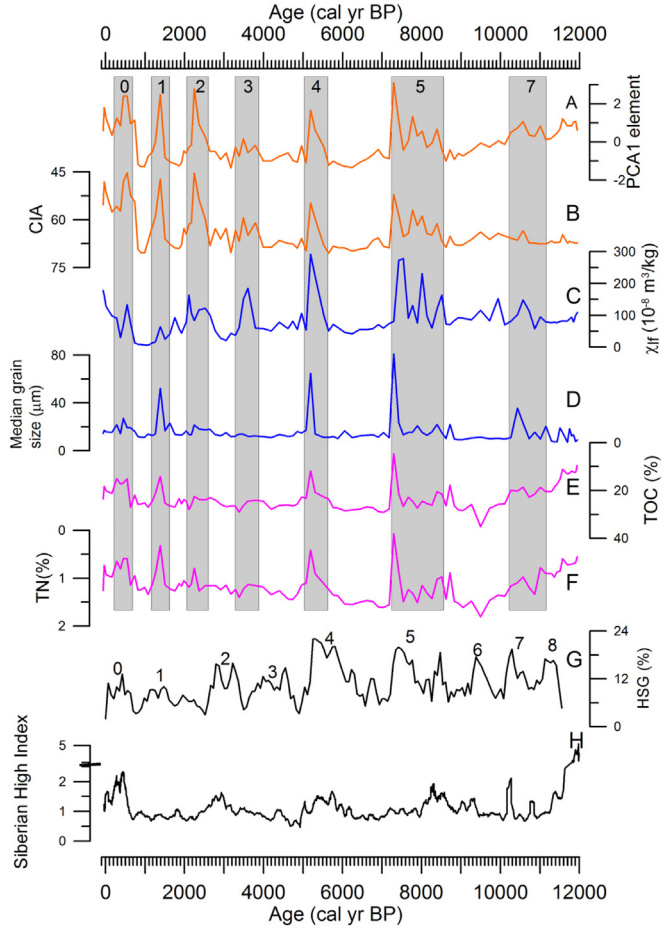

Fig. 7. Short-term oscillations in sedimentary proxies from Tiancai Lake (A–F) in comparison with global climatic records (G–H). (A) Element sample scores on PCA axis 1; (B) chemical index of alteration (CIA); (C) magnetic susceptibility (Han et al., 2011); (D) median grain size (Han et al., 2011); (E) total organic carbon (Chen et al., 2014); (F) total nitrogen (Chen et al., 2014), expressed on the timescale used in this study. (G) Hematite-stained grain (%) in the eastern North Atlantic (MC52-VM29-191; Bond et al., 2001). (H) Siberian High index based on potassium ion content (K^+; ppb) proxy from Greenland ice cores at GIPS2 after an adjacent-averaging smoothing (100 years) (Mayewski et al., 2004). The grey bars indicate the timing of seven Bond-like cooling events during the Holocene.

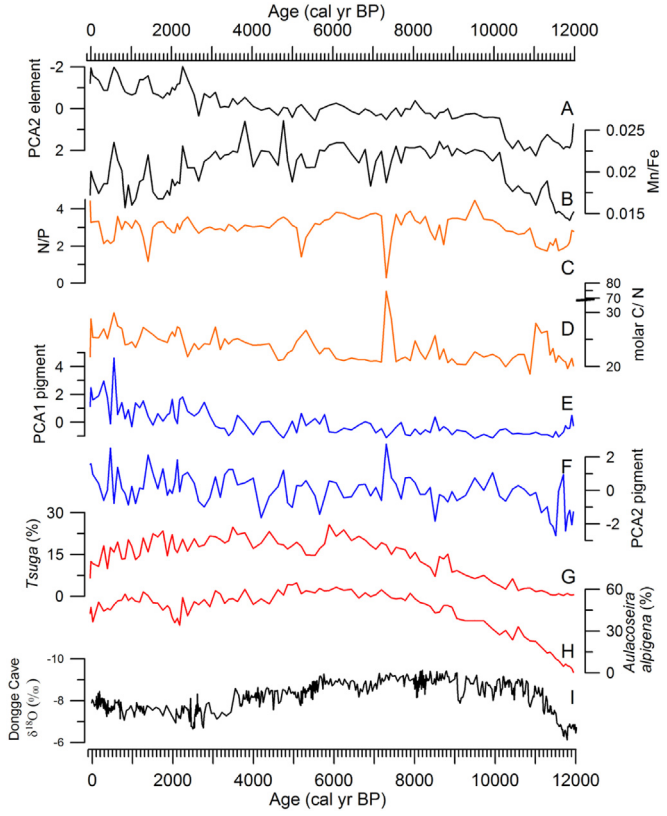

Fig. 8. Long-term changes in sedimentary proxies from Tiancai Lake (A–H) in comparison with global climatic records (I). (A) Element sample scores on PCA2; (B) the ratios of manganese to iron (Mn/Fe); (C) the ratios of nitrogen to phosphorus (N/P); (D) the molar ratios of carbon to nitrogen (C/N); (E) pigment sample scores on PCA 1; (F) pigment sample scores on PCA 2; (G) percentage of *Tsuga* in pollen assemblage (Xiao et al., 2014); (H) percentage of *A. alpigena* in diatom assemblage (Chen et al., 2014), expressed against the age-depth model used in this study; and (I) $\delta^{18}O$ record from Dongge Cave (Dykoski et al., 2005).

cooling events (Fig. 7G).

$PCA2_{elements}$ showed a declining trend, whereas $PCA1_{pigments}$ increased gradually (Fig. 8A and E). Mn/Fe ratio increased in the early Holocene, maintained high values in the middle Holocene, and declined in the late Holocene (Fig. 8B). The broad trend in Mn/Fe is paralleled

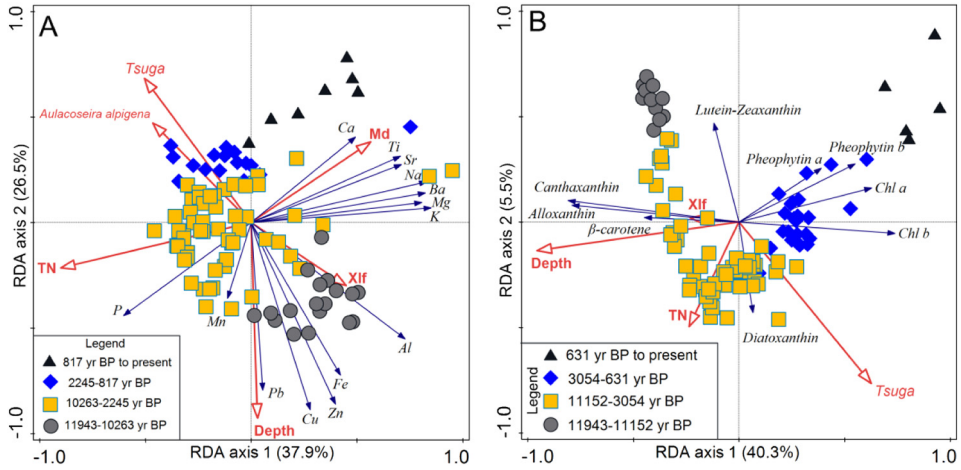

Fig. 9. Biplot of redundancy analysis, (A) elements and significant explanatory variables (four zones correspond to those in Fig. 4) and (B) pigments and significant explanatory variables (four zones correspond to those in Fig. 5).

Table 1
The variance in element/pigment data explained by the unique effect of each significant explanatory variable.

Response variable	Explanatory variable	Indicative significance	Variance explained (%)	*p*-Value
Elements	Sediment depth	Lake infilling	7.3	0.002
	Tsuga	Forest development	5.9	0.002
	Aulacoseira alpigena	Lake alkalinity	2.5	0.002
	TN	Soil development	3.7	0.002
	Md	Erosion	1.3	0.008
	χ_{lf}	Erosion	3.9	0.002
Pigments	Sediment depth	Lake infilling	15.8	0.002
	Tsuga	Forest development	5.7	0.002
	χ_{lf}	Erosion	2.6	0.002
	TN	Soil development	1.7	0.008

by major changes in tree pollen (*Tsuga*), diatom species (*A. alpigena*) and Dongge Cave $\delta^{18}O$ values (Fig. 8).

RDA results revealed that changes in elemental composition were significantly correlated with median grain size (Md), magnetic susceptibility (χ_{lf}), *Tsuga*, *A. alpigena*, TN and sediment depth (Fig. 9A and Table 1). Meanwhile, *Tsuga*, TN, χ_{lf} and sediment depth formed the minimum subset of significant variables for explaining the variance in pigment data (Fig. 9B and Table 1).

4. Discussion

The impacts of Holocene climate changes on ecosystem processes in Tiancai Lake can be summarised using a schematic diagram (Fig. 10). Further description is given in the following sections.

4.1. Catchment soil formation

Low TOC and TN contents but high concentrations of minerogenic elements in the basal samples probably reflected the organically poor and mineral-rich soil in the alpine meadow around Tiancai Lake before ~11 cal kyr B.P. High P concentration in the early part of the record (before ~10 cal kyr B.P.) might have resulted from rich leachable P (e.g., apatite) and high supply rate of P from the treeless catchment (cf. Boyle, 2007). Since ~10 cal kyr B.P., evergreen trees expanded in montane regions (SW China) due to the intensified summer monsoon, suggested by rising *Tsuga* percentage in the pollen records from Tiancai Lake (Xiao et al., 2014), Lugu Lake (Wang et al., 2016a) and Chenghai

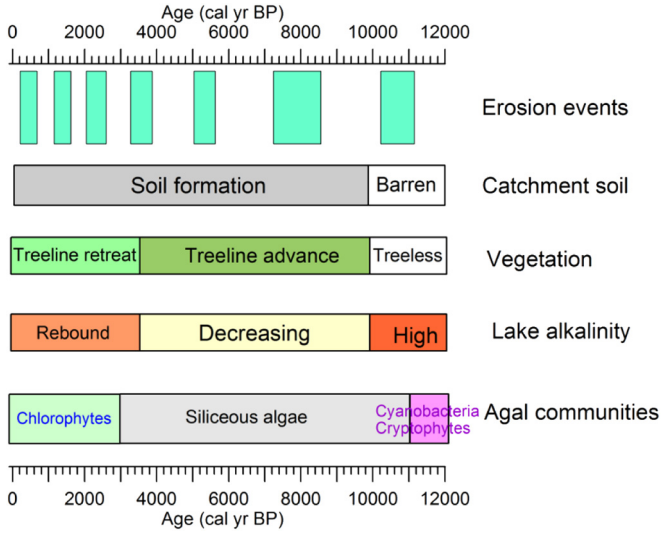

Fig. 10. A schematic diagram of environmental changes in Tiancai Lake during the past 12 ka. Vegetation in the catchment of Tiancai Lake sourced from Xiao et al. (2014). Lake alkalinity accessed from Chen et al. (2014).

Lake (Xiao et al., 2017). Forest development can stabilize soils and gradually reduce inorganic inputs to lakes (Ford, 1990; Hu et al., 1993). For instance, the mobilization of Al, Pb, Cu and Zn from soil A horizons would occur during soil podsolization, with these elements typically deposited lower in the soil profile forming a spodic horizon (cf. Ford, 1990). As a consequence of declining supply from the catchment, Al, Pb, Cu and Zn decreased progressively in lake sediments after ~10 cal kyr B.P.

Meanwhile, increased litter fall from trees would have increased soil humic content, elevated soil acidity, and decreased soil aeration (Hu et al., 1993). Under anoxic conditions, both Mn and Fe may be expected to become mobilized and to pass into solution; a more rapid reduction of Mn than Fe causes preferential Mn release (Mackereth, 1966; Naeher et al., 2013). Increasing Mn/Fe ratios from the early- to mid-Holocene could be linked to preferential removal of Mn from catchment soils, probably due to the onset of reducing conditions in the soils of sufficient intensity to produce Mn^{2+} but not intense enough to generate Fe^{2+} (Mackereth, 1966). Due to strengthened monsoon intensity since the early Holocene, faster lake flushing and so less bottom water anoxia could account for increasing Mn/Fe ratios further (Naeher et al., 2013). In addition, sedimentary P retained relatively high values for several thousand years (from ~10 to 2 cal kyr B.P.), probably resulting from

high sedimentation efficiency from co-precipitation with oxidizing Fe and Mn within lake and biological sedimentation by phytoplankton (Mackereth, 1966). Sedimentary phosphorus content in Tiancai Lake (ranging from 1.98 to 5.14 mg g^{-1}) is relatively higher than that in other lakes from Yunnan Province (ranging from 0.68 to 2.1 mg g^{-1}) (Whitmore et al., 1997).

Declining TN and TOC contents after ~3 cal kyr B.P. implied soil thinning due to forest retreat (Xiao et al., 2014), which will in turn weaken reducing conditions in catchment soils and limit the migration of Fe and Mn, revealed by general decreases in Fe and Mn. Besides the general trend, several peaks in Mn/Fe ratios were likely linked to the separation of Fe and Mn during erosional transport (cf. Mackereth, 1966). PCA $2_{elements}$ was positively correlated with Al, Pb, Cu and Zn, Mn, Fe and P (Fig. 6A), indicating that PCA $2_{elements}$ mainly reflect surrounding soil development.

4.2. Episodic erosion events

Synchronous peaks in minerogenic elements (i.e., Ti, Ba, Ca, Sr, Na, K and Mg), median grain size and magnetic susceptibility coincided with troughs in CIA values (Figs. 4 and 7), indicative of high intensity of freeze-thaw processes that removed unleached and coarse detritus materials before the processes of chemical attack had time to be fully effective (Mackereth, 1966; Boyle, 2001). These erosion events, likely linked to prolonged ice-cover and ice-melt duration in the catchment (Schmidt et al., 2006), could transport detritus materials directly into the lake by meltwater inflow and slope wash (Pennington et al., 1972; Solovieva and Jones, 2002). Positive correlations between PCA $1_{element}$ and these minerogenic elements suggested that PCA $1_{element}$ mainly represent the erosion intensity of upland bedrock.

These strong erosion events, within dating error, may be coincident with Holocene cold events recorded in lake sediments, peats and ice cores from the Tibetan Plateau and adjacent montane regions (see the review by Mischke and Zhang, 2010), as well as Holocene ice-rafting events in the North Atlantic (Fig. 7G). For example, the cold spell between 8.5 and 7.2 cal kyr B.P. was inferred also from other sites located in the eastern Tibetan Plateau, including Hongyuan Peatland (Hong et al., 2003), Naleng Lake (Kramer et al., 2010) and Ximencuo Lake (Mischke and Zhang, 2010). The cold events in the North Atlantic region, which resulted from changes in external solar forcing (Wang et al., 2005) and internal oceanic and atmospheric circulation (Darby et al., 2012), could influence the East Asian winter monsoon probably through the impact of the Siberian High (Gong et al., 2001; Fig. 7H). In addition, the orographically-derived features of the Tibetan Plateau (e.g., an extended snow-cover period) and catchment-specific response (e.g., steep topography) of the lake system could enhance the impacts of these cold events (Kramer et al., 2010; Mischke and Zhang, 2010; Anderson et al., 2012). For instance, the steep and rugged topography of the Tiancai Lake catchment could facilitate upland bedrock weathering by the freeze-thaw process because of the sharp gradients in climatic parameters (e.g., temperature and radiation) over very short distances (Brisset et al., 2013). Further research is needed to investigate a denser network of paleoclimate records in the Tibetan Plateau to more clearly evaluate the spatial pattern of these short-term events and thus to elucidate their potential drivers.

4.3. Changes in algal community structure

High abundances of cyanobacteria and cryptophytes during the early Holocene were positively correlated with sediment depth (Fig. 9B), indicating that they may be influenced by lake water depth. Sediment infilling has gradually reduced lake depth by ca. 9 m over the last 12 kyr. Both cyanobacteria and cryptophytes are suited to deeper lakes which stratify, due to their ability to alter their depth position in the water column to optimise access to nutrients (P and N). Cyanobacteria are also particularly prevalent in alkaline environments, with abundant minerals and phosphorus from the treeless catchment (McGowan et al., 2008; Reuss et al., 2010). In addition, they are known to be well suited to cold environments (Leavitt and Findlay, 1994; Lotter, 2001).

With vegetation and soil development from ca. 11 cal kyr B.P., microbial nitrogen fixation in soils would be enhanced by early successional plants (Fritz et al., 2004), such as *Alnus* around Tiancai Lake (Xiao et al., 2014). After nitrogen mineralization during winter, substantial inorganic nitrogen is exported from terrestrial systems during the snowmelt season, when terrestrial plants are unable to utilize the plant available N pool (Fritz and Anderson, 2013). Increasing nitrogen supply, suggested by rising TN contents and N/P ratios (Figs. 7F and 8C), would favour siliceous algae over cyanobacteria in the lake (Cross et al., 2014; Fig. 9B). Meanwhile, an increasing influx of dissolved organic matter from terrestrial sources, indicated by rising TOC content, might have reduced the light availability and alkalinity of the lake water (Williamson et al., 1999; Engstrom et al., 2000). Present monitoring data revealed that the concentration of DOC was moderately high in Tiancai Lake (~10 mg L^{-1}). Such conditions are highly suited to cryptophytes, which persisted at this time as they are able to employ mixotrophy to utilize organic carbon sources (Lepistö and Rosenström, 1998). Cryptophytes and other siliceous algae groups such as chrysophytes are common in dystrophic lakes (Jones et al., 2011). Despite a weakening of the monsoon intensity after the mid-Holocene (Dykoski et al., 2005), no directional trends in pigment concentrations indicated relatively stable algal communities for the timespan from ~7 to 3 cal kyr B.P., probably due to replete supplies of phosphorus and nitrogen.

The most marked transition around 3 cal kyr B.P., i.e., substantial increases in pigments from chlorophytes/aquatic plants and obvious decreases in cyanobacteria and cryptophytes, signified a major ecological shift in Tiancai Lake. A return to relatively dry and cold climatic conditions in the late Holocene led to the replacement of trees (*Tsuga*) by shrubs (Ericaceae) and surface runoff reduction in the catchment (Chen et al., 2014; Xiao et al., 2014). As a consequence, reducing tree canopy in the littoral zone and declining supply of terrestrial organic matter to the lake could increase light penetration depths. Coupled with decreasing water depths due to sediment infilling, this probably expanded benthic production in the lake. Accordingly the pigments indicate increased production of (benthic) chlorophytes, or aquatic macrophytes (each indicated by the pigments Chl *b* and pheophytin *b*) (Reuss et al., 2010). A slight increase in C/N ratios after ~3 cal kyr B.P. (Fig. 8D) probably indicated a rising contribution of macrophytes (Meyers and Ishiwatari, 1993). Further increase in Chl *b* and pheophytin *b* after ~541 cal yr B.P. denoted favourable light and nutrient conditions for chlorophytes, since the vast majority of chlorophytes are autotrophic (Wehr et al., 2015). Algal growth tends to deplete the carbon dioxide in water column, probably accounting for moderate pH in Tiancai Lake.

4.4. The links between catchment and lake processes

Both pigment and elemental data were significantly correlated with TN (catchment soil), χ_{lf} (erosion), *Tsuga* (vegetation) and sediment depth (lake infilling) (Fig. 9A–B), highlighting direct and indirect effects of Holocene climate variations on lake ecosystem evolution. For instance, the peaks of minerogenic elements (i.e., Ti, Ba, Ca, Sr, Na, K and Mg) mainly responded to prolonged ice-cover period and enhanced physical weathering during cold events, while the decrease in cyanobacteria was partly linked to lake infilling since the early Holocene. Despite several erosion events in Tiancai Lake catchment, there were subtle responses of algal communities to these erosion processes, suggested by weak correlations between pigment data and PCA $1_{elements}$ (an indicator for erosion intensity; Fig. 11A–B). In contrast, pigment data were highly correlated with PCA $2_{elements}$ (a proxy for soil development; Fig. 11C–D). The results denoted that direct responses of algae

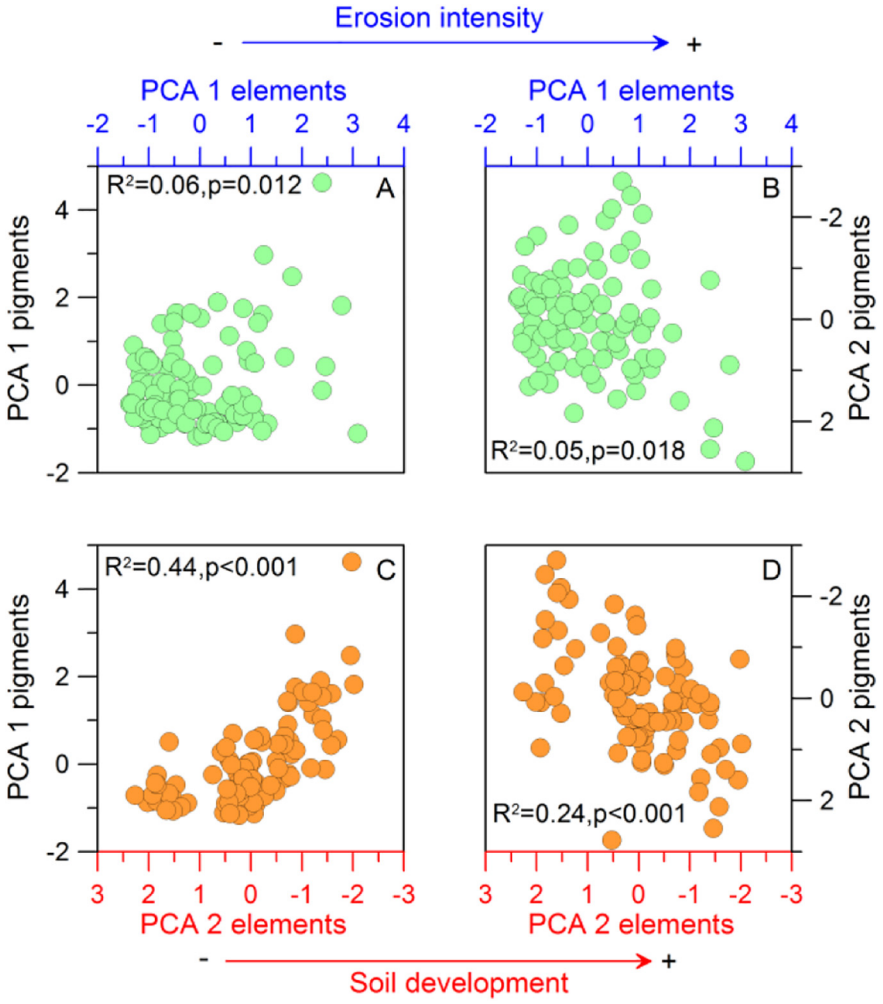

Fig. 11. Correlation relationships between pigment and element data, including PCA1$_{elements}$ and PCA 1$_{pigments}$ (A), PCA 1$_{elements}$ and PCA 2$_{pigments}$ (B), PCA 2$_{elements}$ and PCA 1$_{pigments}$ (C), and PCA 2$_{elements}$ and PCA 2$_{pigments}$ (D).

to short-term climatic oscillations are overridden by strong catchment-lake interactions. Specifically, in this region where sources of P (from bedrock weathering) and N (from soil development) have been replete for much of the Holocene, there are only subtle changes in overall primary producer abundance, with the most marked effects later in the record being caused by internal (lake infilling) processes.

During cold events, clastic materials are produced by bedrock weathering and transported annually in to the lake by melt-waters in the spring (Fig. 12). Meanwhile, percolation of melt-water through paludified soil supplied solutes (e.g., phosphorus and nitrogen) to this lake and helped to maintain relatively stable limnological conditions for algae during the growth season (Catalan et al., 2013). Feedback mechanisms operate effectively whereby changes in limnological conditions (e.g., an increase in alkalinity) due to strong erosion can be inhibited by buffering processes in catchment soils (Fig. 12).

In addition, both element and pigment data were significantly correlated with sediment depth, highlighting the strong influence of lake infilling on the lake. The natural progressive infilling due to gradual accumulation of terrestrial and autochthonous materials leads to lake shallowing and littoral zone expansion, conforming to models of lake ontogeny (Binford et al., 1983). As a consequence, the development of benthic chlorophytes and aquatic macrophytes contributed to the increases in Chl *b* and pheophytin *b* in the late Holocene. Meanwhile, lake volume loss would shorten water retention time, indirectly altering sedimentation rate and redox condition in the water column. Hence, lake infilling could interact with climatic variations and catchment processes, influencing algal community structure and geochemical processes in Tiancai Lake.

5. Conclusions

Sedimentary pigments and elements in Tiancai Lake were analysed to reveal the co-evolution of catchment and lake ecosystems in response to Holocene climate variations. High abundances of cyanobacteria and cryptophytes in the early Holocene were related to alkaline conditions after the deglaciation, and relatively stable algal communities in the mid-Holocene was followed by the expansion of chlorophytes and/or aquatic plants in the late Holocene. Al, Zn, Cu and Pb decreased generally from the early Holocene, mainly in response to soil development. Changes in Mn and Fe were related to redox condition dynamics in catchment soils and the water column. Peaks in Ti, Ba, Ca, Sr, Na, K and Mg signified erosion events and the influxes of unleached particles and base cations. Despite several erosion events, the rather subtle variations in algal communities were probably linked to replete nutrient supply from catchment soils. The catchment can filter the direct effects of climate on lakes, because local bedrock, topography, soils and vegetation alter runoff and mass transfer from land to water. Overall, this study provides well-dated pigment and element records in an alpine lake during the Holocene, underscoring strong co-evolutionary relationships between climate, vegetation, soil development, lake infilling and algal communities.

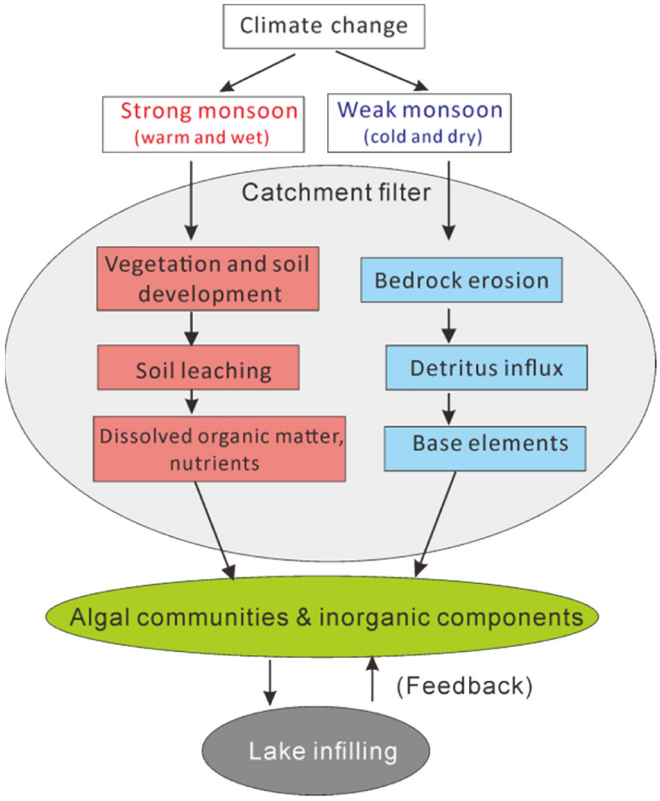

Fig. 12. Representation of catchment and lake processes in response to Holocene climate variations.

Acknowledgments

We thank Teresa Needham, Graham Morris, Qianglong Qiao and Yuxin Zhu for help with laboratory analyses. This work was supported by National Key R&D Program of China (2016YFA0600501), the National Natural Science Foundation of China (41572149, 41572343), and the Fundamental Research Fund for National University, China University of Geosciences, Wuhan (G1323511656). Xu Chen was supported by a Postdoctoral Scholarship of the China Scholarship Council (201206415008).

References

Anderson, N.J., Liversidge, A.C., McGowan, S., Jones, M.D., 2012. Lake and catchment response to Holocene environmental change: spatial variability along a climate gradient in southwest Greenland. J. Paleolimnol. 48 (1), 209–222.
Battarbee, R., Thompson, R., Catalan, J., Grytnes, J.-A., Birks, H.J.B., 2002. Climate variability and ecosystem dynamics of remote alpine and arctic lakes: the MOLAR project. J. Paleolimnol. 28 (1), 1–6.
Bennett, K.D., 1996. Determination of the number of zones in a biostratigraphical sequence. New Phytol. 132 (1), 155–170.
Binford, M.W., Deevey, E.S., Crisman, T.L., 1983. Paleolimnology: an historical perspective on lacustrine ecosystems. Annu. Rev. Ecol. Evol. Syst. 14 (1), 255–286.
Blaauw, M., Christen, J.A., 2011. Flexible paleoclimate age-depth models using an autoregressive gamma process. Bayesian Anal. 6 (3), 457–474.
Bond, G., Kromer, B., Beer, J., Muscheler, R., Evans, M.N., Showers, W., Hoffmann, S., Lotti-Bond, R., Hajdas, I., Bonani, G., 2001. Persistent solar influence on North Atlantic climate during the Holocene. Science 294 (5549), 2130–2136.
Boyle, J., Chiverrell, R., Plater, A., Thrasher, I., Bradshaw, E., Birks, H., Birks, J., 2013. Soil mineral depletion drives early Holocene lake acidification. Geology 41 (4), 415–418.
Boyle, J.F., 2001. Inorganic geochemical methods in palaeolimnology. In: Last, W.M., Smol, J.P. (Eds.), Tracking Environmental Change Using Lake Sediments: Physical and Geochemical Methods. Springer Netherlands, Dordrecht, pp. 83–141.
Boyle, J.F., 2007. Loss of apatite caused irreversible early-Holocene lake acidification. The Holocene 17 (4), 543–547.
Bradshaw, E.G., Jones, V.J., Birks, H.J.B., Birks, H., 2000. Diatom responses to late-glacial and early-Holocene environmental changes at Kråkenes, western Norway. J. Paleolimnol. 23 (1), 21–34.
Brisset, E., Miramont, C., Guiter, F., Anthony, E.J., Tachikawa, K., Poulenard, J., Arnaud, F., Delhon, C., Meunier, J.-D., Bard, E., Suméra, F., 2013. Non-reversible geosystem destabilisation at 4200 cal. BP: Sedimentological, geochemical and botanical markers of soil erosion recorded in a Mediterranean alpine lake. The Holocene 23 (12), 1863–1874.
Catalan, J., Pla-Rabés, S., Wolfe, A., Smol, J., Rühland, K., Anderson, N.J., Kopáček, J., Stuchlík, E., Schmidt, R., Koinig, K., Camarero, L., Flower, R., Heiri, O., Kamenik, C., Korhola, A., Leavitt, P., Psenner, R., Renberg, I., 2013. Global change revealed by palaeolimnological records from remote lakes: a review. J. Paleolimnol. 49 (3), 513–535.
Chen, N., Bianchi, T.S., McKee, B.A., Bland, J.M., 2001. Historical trends of hypoxia on the Louisiana shelf: application of pigments as biomarkers. Org. Geochem. 32 (4), 543–561.
Chen, X., Li, Y., Metcalfe, S., Xiao, X., Yang, X., Zhang, E., 2014. Diatom response to Asian monsoon variability during the Late Glacial to Holocene in a small treeline lake, SW China. The Holocene 24 (10), 1369–1377.
Cross, I.D., McGowan, S., Needham, T., Pointer, C.M., 2014. The effects of hydrological extremes on former gravel pit lake ecology: management implications. Fundam. Appl. Limnol. 185 (1), 71–90.
Darby, D.A., Ortiz, J.D., Grosch, C.E., Lund, S.P., 2012. 1,500-year cycle in the Arctic Oscillation identified in Holocene Arctic sea-ice drift. Nat. Geosci. 5 (12), 897–900.
Du, Y., Zhang, Y., Chen, F., Chang, Y., Liu, Z., 2016. Photochemical reactivities of dissolved organic matter (DOM) in a sub-alpine lake revealed by EEM-PARAFAC: an insight into the fate of allochthonous DOM in alpine lakes affected by climate change. Sci. Total Environ. 568, 216–225.
Dykoski, C.A., Edwards, R.L., Cheng, H., Yuan, D.X., Cai, Y.J., Zhang, M.L., Lin, Y.S., Qing, J.M., An, Z.S., Revenaugh, J., 2005. A high-resolution, absolute-dated Holocene and deglacial Asian monsoon record from Dongge Cave, China. Earth Planet. Sci. Lett. 233 (1–2), 71–86.
Engstrom, D.R., Fritz, S.C., Almendinger, J.E., Juggins, S., 2000. Chemical and biological trends during lake evolution in recently deglaciated terrain. Nature 408 (6809), 161–166.
Ford, M.S., 1990. A 10,000-yr history of natural ecosystem acidification. Ecol. Monogr. 60 (1), 57–89.
Fritz, S.C., Anderson, N.J., 2013. The relative influences of climate and catchment processes on Holocene lake development in glaciated regions. J. Paleolimnol. 49 (3), 349–362.
Fritz, S.C., Engstrom, D.R., Juggins, S., 2004. Patterns of early lake evolution in boreal landscapes: a comparison of stratigraphic inferences with a modern chronosequence in Glacier Bay, Alaska. The Holocene 14 (6), 828–840.
Gong, D.Y., Wang, S.W., Zhu, J.H., 2001. East Asian winter monsoon and Arctic Oscillation. Geophys. Res. Lett. 28 (10), 2073–2076.
Grimm, E., 1991. TILIA Version 1.11. TILIAGRAPH Version 1.18. A Users Notebook. Illinois State Museum, Springfield, USA.
Han, Y., Xiao, X., Yang, X., Zhang, E., Xiao, J.Y., 2011. The grain-size characteristics of Tiancai Lake in northwestern of Yunnan Province and paleo-precipitation history during the Holocene. Quat. Res. 31, 999–1010 (in Chinese).
Hong, Y.T., Hong, B., Lin, Q.H., Zhu, Y.X., Shibata, Y., Hirota, M., Uchida, M., Leng, X.T., Jiang, H.B., Xu, H., Wang, H., Yi, L., 2003. Correlation between Indian Ocean summer monsoon and North Atlantic climate during the Holocene. Earth Planet. Sci. Lett. 211 (3–4), 371–380.
Hu, F.S., Brubaker, L.B., Anderson, P.M., 1993. A 12000 year record of vegetation change and soil development from Wien Lake, central Alaska. Can. J. Bot. 71 (9), 1133–1142.
Jones, V.J., Solovieva, N., Self, A.E., McGowan, S., Rosen, P., Salonen, J.S., Seppa, H., Valiranta, M., Parrott, E., Brooks, S.J., 2011. The influence of Holocene tree-line advance and retreat on an arctic lake ecosystem: a multi-proxy study from Kharinei Lake, North Eastern European Russia. J. Paleolimnol. 46 (1), 123–137.
Koinig, K.A., Shotyk, W., Lotter, A.F., Ohlendorf, C., Sturm, M., 2003. 9000 years of geochemical evolution of lithogenic major and trace elements in the sediment of an alpine lake – the role of climate, vegetation, and land-use history. J. Paleolimnol. 30 (3), 307–320.
Kramer, A., Herzschuh, U., Mischke, S., Zhang, C., 2010. Holocene treeline shifts and monsoon variability in the Hengduan Mountains (southeastern Tibetan Plateau), implications from palynological investigations. Palaeogeogr. Palaeoclimatol. Palaeoecol. 286 (1), 23–41.
Leavitt, P., Hodgson, D., 2001. Sedimentary pigments. In: Smol, J., Birks, H.J., Last, W., Bradley, R., Alverson, K. (Eds.), Tracking Environmental Change Using Lake Sediments. Developments in Paleoenvironmental Research, vol. 3. Springer Netherlands, pp. 295–325.
Leavitt, P.R., Findlay, D.L., 1994. Comparison of fossil pigments with 20 years of phytoplankton data from eutrophic Lake-227, experimental lakes area, Ontario. Can. J. Fish. Aquat. Sci. 51 (10), 2286–2299.
Leavitt, P.R., Fritz, S.C., Anderson, N.J., Baker, P.A., Blenckner, T., Bunting, L., Catalan, J., Conley, D.J., Hobbs, W.O., Jeppesen, E., Korhola, A., McGowan, S., Ruhland, K., Rusak, J.A., Simpson, G.L., Solovieva, N., Werne, J., 2009. Paleolimnological evidence of the effects on lakes of energy and mass transfer from climate and humans. Limnol. Oceanogr. 54 (6), 2330–2348.
Lepistö, L., Rosenström, U., 1998. The most typical phytoplankton taxa in four types of boreal lakes. Hydrobiologia 369 (0), 89–97.
Li, Y., Chen, X., Xiao, X., Zhang, H., Xue, B., Shen, J., Zhang, E., 2018. Diatom-based inference of Asian monsoon precipitation from a volcanic lake in southwest China for the last 18.5 ka. Quat. Sci. Rev. 182, 109–120.
Likens, G.E., Bormann, F.H., 1974. Linkages between terrestrial and aquatic ecosystems. Bioscience 24 (8), 447–456.
Lotter, A., 2001. The palaeolimnology of Soppensee (Central Switzerland), as evidenced by diatom, pollen, and fossil-pigment analyses. J. Paleolimnol. 25 (1), 65–79.

Lotter, A.F., Birks, H.J.B., 2003. The Holocene palaeolimnology of Sägistalsee and its environmental history – a synthesis. J. Paleolimnol. 30 (3), 333–342.
Lu, Y., Fritz, S.C., Stone, J.R., Krause, T.R., Whitlock, C., Brown, E.T., Benes, J.V., 2017. Trends in catchment processes and lake evolution during the late-glacial and early- to mid-Holocene inferred from high-resolution XRF data in the Yellowstone region. J. Paleolimnol. 58 (4), 551–569.
Ma, H.H., 2013. Petrology and Geochemical Characteristics of Laojunshan Granite in Southeast Yunnan and Its Tectonic Significance (Master thesis). China University of Geosciences (Beijing), Beijing, China (in Chinese).
Mackereth, F.J.H., 1966. Some chemical observations on post-glacial lake sediments. Philos. Trans. R. Soc. Lond. Ser. B Biol. Sci. 250 (765), 165–213.
Mayewski, P.A., Rohling, E.E., Stager, J.C., Karlen, W., Maasch, K.A., Meeker, L.D., Meyerson, E.A., Gasse, F., van Kreveld, S., Holmgren, K., Lee-Thorp, J., Rosqvist, G., Rack, F., Staubwasser, M., Schneider, R.R., Steig, E.J., 2004. Holocene climate variability. Quat. Res. 62 (3), 243–255.
McGowan, S., 2013. Paleolimnology | Pigment studies. In: Elias, S.A., Mock, C.J. (Eds.), Encyclopedia of Quaternary Science, Second Edition. Elsevier, Amsterdam, pp. 326–338.
McGowan, S., Juhler, R.K., Anderson, N.J., 2008. Autotrophic response to lake age, conductivity and temperature in two West Greenland lakes. J. Paleolimnol. 39 (3), 301–317.
Meyers, P.A., Ishiwatari, R., 1993. Lacustrine organic geochemistry—an overview of indicators of organic matter sources and diagenesis in lake sediments. Org. Geochem. 20 (7), 867–900.
Mischke, S., Zhang, C., 2010. Holocene cold events on the Tibetan Plateau. Glob. Planet. Chang. 72 (3), 155–163.
Morrill, C., Overpeck, J.T., Cole, J.E., 2003. A synthesis of abrupt changes in the Asian summer monsoon since the last deglaciation. The Holocene 13 (4), 465–476.
Naeher, S., Gilli, A., North, R.P., Hamann, Y., Schubert, C.J., 2013. Tracing bottom water oxygenation with sedimentary Mn/Fe ratios in Lake Zurich, Switzerland. Chem. Geol. 352, 125–133.
Nesbitt, H.W., Young, G.M., 1982. Early proterozoic climates and plate motions inferred from major element chemistry of lutites. Nature 299 (5885), 715–717.
Ning, D., Zhang, E., Sun, W., Chang, J., Shulmeister, J., 2017. Holocene Indian Summer Monsoon variation inferred from geochemical and grain size records from Lake Ximenglongtan, southwestern China. Palaeogeogr. Palaeoclimatol. Palaeoecol. 487, 260–269.
Pennington, W., Tutin, T.G., Haworth, E., Bonny, A.P., Lishman, J.P., 1972. Lake sediments in northern Scotland. Philos. Trans. R. Soc. Lond. Ser. B Biol. Sci. 264 (861), 191–294.
Renberg, I., 1990. A 12600 year perspective of the acidification of Lilla Oresjon, southwest Sweden. Philos. Trans. R. Soc. Lond. Ser. B Biol. Sci. 327 (1240), 357–361.
Reuss, N.S., Hammarlund, D., Rundgren, M., Segerstrom, U., Eriksson, L., Rosen, P., 2010. Lake ecosystem responses to Holocene climate change at the subarctic tree-line in northern Sweden. Ecosystems 13 (3), 393–409.
Schmidt, R., Kamenik, C., Tessadri, R., Koinig, K.A., 2006. Climatic changes from 12,000 to 4,000 years ago in the Austrian Central Alps tracked by sedimentological and biological proxies of a lake sediment core. J. Paleolimnol. 35 (3), 491–505.
Shi, J.P., 2007. Community Ecology and Biogeography of the Mossy Dwarf Forest in Yunnan (PhD thesis). Xishuangbanna Tropical Botanical Garden, Chinese Academy of Sciences, Kunming, China (in Chinese).
Šmilauer, P., Lepš, J., 2014. Multivariate Analysis of Ecological Data Using CANOCO 5, 2 ed. Cambridge University Press, Cambridge.
Solovieva, N., Jones, V.J., 2002. A multiproxy record of Holocene environmental changes in the central Kola Peninsula, northwest Russia. J. Quat. Sci. 17 (4), 303–318.
Wang, Q., Yang, X., Anderson, N.J., Dong, X., 2016a. Direct versus indirect climate controls on Holocene diatom assemblages in a sub-tropical deep, alpine lake (Lugu Hu, Yunnan, SW China). Quat. Res. 86, 1):1–12.
Wang, X., Chu, G., Sheng, M., Zhang, S., Li, J., Chen, Y., Tang, L., Su, Y., Pei, J., Yang, Z., 2016b. Millennial-scale Asian summer monsoon variations in South China since the last deglaciation. Earth Planet. Sci. Lett. 451, 22–30.
Wang, Y., Cheng, H., Edwards, R.L., He, Y., Kong, X., An, Z., Wu, J., Kelly, M.J., Dykoski, C.A., Li, X., 2005. The Holocene Asian monsoon: links to solar changes and North Atlantic climate. Science 308 (5723), 854–857.
Wehr, J.D., Sheath, R.G., Kociolek, J.P., 2015. Freshwater Algae of North America: Ecology and Classification. Elsevier.
Whitmore, T.J., Brenner, M., Jiang, Z., Curtis, J.H., Moore, A.M., Engstrom, D.R., Wu, Y., 1997. Water quality and sediment geochemistry in lakes of Yunnan Province, southern China. Environ. Geol. 32 (1), 45–55.
Williamson, C.E., Morris, D.P., Pace, M.L., Olson, O.G., 1999. Dissolved organic carbon and nutrients as regulators of lake ecosystems: resurrection of a more integrated paradigm. Limnol. Oceanogr. 44 (3), 795–803.
Xiao, X., Haberle, S.G., Li, Y., Liu, E., Shen, J., Zhang, E., Yin, J., Wang, S., 2017. Evidence of Holocene climatic change and human impact in northwestern Yunnan Province: high-resolution pollen and charcoal records from Chenghai Lake, southwestern China. The Holocene 28 (1), 127–139.
Xiao, X., Haberle, S.G., Shen, J., Yang, X., Han, Y., Zhang, E., Wang, S., 2014. Latest Pleistocene and Holocene vegetation and climate history inferred from an alpine lacustrine record, northwestern Yunnan Province, southwestern China. Quat. Sci. Rev. 86 (0), 35–48.
Zhang, E., Chang, J., Cao, Y., Sun, W., Shulmeister, J., Tang, H., Langdon, P.G., Yang, X., Shen, J., 2017. Holocene high-resolution quantitative summer temperature reconstruction based on subfossil chironomids from the southeast margin of the Qinghai-Tibetan Plateau. Quat. Sci. Rev. 165, 1–12.